Turkish Journal of Electrical Engineering & Computer Sciences

http://journals.tubitak.gov.tr/elektrik/

Research Article

Turk J Elec Eng & Comp Sci
(2016) 24: 1034 – 1043

doi:10.3906/elk-1309-95

Optimization with genetic algorithm of temperature-dependent fiber length of L-band EDFA gain

Murat YÜCEL[1,*], **Damt ADNAN MUSTAFA MUSTAFA**[2]

[1]Department of Electrical-Electronics Engineering, Faculty of Technology, Gazi University, Teknikokullar, Ankara, Turkey

[2]Department of Electronics Computer Education, Information Institute, Gazi University, Teknikokullar, Ankara, Turkey

Received: 12.09.2013 • **Accepted/Published Online:** 01.02.2014 • **Final Version:** 23.03.2016

Abstract: Erbium-doped fiber amplifiers (EDFAs) have great importance in long-distance communication. It is required to have equal gain for all signals that are transferred and to avoid loss in the receiver of long-distance communication systems. However, temperature dependence changes the output spectrum of the designed gain-flattening systems. In this study, each erbium-doped fiber (EDF) length of a two-stage L-band EDFA has been optimized using a genetic algorithm method; because of the temperature dependence of EDFAs, there is no general rule. Thus, a simple, fast, dynamic, and highly accurate model has been developed and obtained for different EDF lengths that will fix gain along the L-band. The results have been shown to be very compatible with the previously obtained numerical values.

Key words: Erbium-doped fiber amplifiers, genetic algorithm, fiber length, optimization

1. Introduction

Optical amplifiers are widely used in long-haul communication systems. They do not require electrical conversation or amplification of light in their own environment. They have both high optical gain and optical bandwidth [1–3]. In addition, optical amplifiers are among very important wavelength division multiplexing (WDM) systems that provide large numbers of signal transmissions in a single fiber. In addition to that, these systems are required for very fast and high-capacity optical communications [4,5]. However, the gain spectrum of optical amplifiers is not flattened and therefore it limits the transmission capacity of WDM systems. Hence, wide-band optical amplifiers with flat gain are being developed. Erbium-doped fiber amplifiers (EDFAs) are among them; they are widely used and have high gain, low noise figure, wide bandwidth, and high efficiency [6–10].

The output gain and the noise figure values of EDFAs have been defined with different methods. However, environmental temperature variations change the stimulated emission and absorption cross-sections of EDFAs and consequently the gain and noise figure values of EDFAs are altered [11–16]. The effect of temperature variations can be addressed by different calculation methods, but there is no exact solution.

Artificial intelligence methods are commonly used in nonlinear systems with no exact solution [17–34]. Therefore, genetic algorithms (GAs) are widely used to solve optimization problems in these methods. In previous studies, Riziotis and Vasilakos analyzed the numerical intelligence applications for the efficient use of

*Correspondence: muyucel@gazi.edu.tr

the bandwidth of fiber optic lines [35]. In another study, Liu and Lee showed that in EDFA and Raman amplifier pump optimization with a GA, higher gain and a higher bandwidth were accomplished [36]. Prudenzano et al. designed EDFAs and lasers using a GA [37]. Cheng and Xiao used a GA for the optimization of EDFAs [38]. Zhang et al. proposed a GA structure for the gain flattening of EDFAs [39]. Kim et al. also used it for the gain flattening of EDFAs [40].

In this study, first and second erbium-doped fiber (EDF) lengths are optimized with a GA to obtain the fixed 25 dB gain output of the two-stage EDFA configuration. In addition, fixed output gain is the same for all wavelengths and all signal powers. In Section 2, theoretical analysis is conducted; methods and materials are described in Section 3 and then the results are discussed.

2. Theoretical analysis

A two-level system is taken into account for the 1480-nm pumped EDFA. Because erbium ions are pumped directly from the ground level, it allows for the metastable level. In addition to analysis of the temperature of each level, we should consider their separation occurring in Stark splitting. Figure 1 shows the separation of these Stark splits [41].

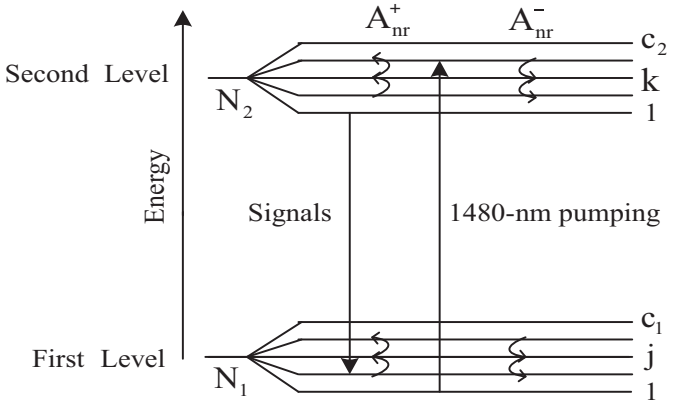

Figure 1. The diagram of energy level of two-level Stark splits.

For all of the energy values of the low and high energy levels, the relative intensities of the possible internal passage vary with respect to the spectral cross-section that is homogeneous and nonhomogeneous. The cross-section only can be found experimentally by measuring because of each level of the number of ions. Einstein analysis that uses the traditional approach of two-level analysis gives the Füchtbauer–Ladenburg relationship:

$$\sigma_i(\nu) = \frac{(\lambda/n)^2 g_i(\nu)}{8\pi\tau}, \tag{1}$$

where λ is wavelength, n is refractive index, τ is ion lifetime and $g(\nu)$ is the line shape function that is the normalized value of the absorption or emission spectrum at frequency ν. Absorption and emission cross-sections of the two-level model of the system must be equal to the upper and lower laser levels, but low Stark is not the case for EDFAs in the lower level.

$$\frac{N_2}{N_1} = \exp\left(-\frac{\Delta E}{k_B T}\right), \tag{2}$$

where k_B is Boltzmann's constant and T is the temperature in Kelvin. In addition, the McCumber theory is an alternative to analysis of the Einstein theory. This theory can be applied at any frequency, and giving a

two-section rate uses the concept of the temperature dependence of the energy. Information about the energy levels can be found in some of the assumptions and predictions. However, they cannot predict the previous section because for the temperature dependence of EDFA there is no general rule [11,42–46].

In Figure 1, each energy is called level 1 and 2, wherein the total orbital momentum is J; $c = J + 1/2$ are the energy sublevels of each separation in several layers, and c indicates the total energy interferences. Maximum Stark separation shows with the main energy levels 1 and 2 a large part of the energy separation between the energy levels [47].

The constant ion distribution continues in various decompositions by the constant temperature effect. Levels 1 and 2 correspond to each of the many layers with a total ion concentration shown as N_1 and N_2. k shows the multilayer index of the lower level of the second energy level ($k = 1, ..., c$), wherein each of the lower level populations is $N_{n,m}$. n shows the laser level of the subindex, and m shows the multilayer.

The thermalization process happening within each manifold is characterized by the nonradiative rates A^+_{nr} and A^-_{nr}, which correspond to the excitation or deexcitation of the ions, with absorption or emission of a phonon. The obtained formula below is under thermal equilibrium:

$$A^-_{nr} N_{nm} = A^+_{nr} N_{n,m-1}. \tag{3}$$

The energy difference between (n, m) and $(n, m-1)$ sublevels is $\Delta E_m = E_m - E_{m-1}$ and the result of $N_{nm}/N_{n,m-1} = A^+_{nr}/A^-_{nr} = \exp(-\Delta E_m/k_B T)$ relation is obtained. Eq. (2.3) is recalculated, obtaining the below relation [41]:

$$N_{nm} = \frac{\exp\left[-(E_m - E_{m-1})/k_B T\right]}{\sum\limits_{m=1}^{c_m} \exp\left[-\left(E_m - E_1\right)/k_B T\right]} \overline{N_n} \equiv p_{nm} \overline{N_n}, \tag{4}$$

where p_{nm} is the Boltzmann distribution. There are many sublevels in the system. However, we investigate the relationship between the first two of these sublevels. Eq. (2.2) is rewritten:

$$\beta = \frac{N_{22}}{N_{21}} = \frac{A^+_{nr}}{A^-_{nr}} = \exp\left(-\frac{\Delta E_2}{k_B T}\right), \tag{5}$$

where N_{21} and N_{22} are Stark splits of the second level (N_2), if E_{22} and E_{21} define the upper and lower level of the sublevels in the metastable level, $\Delta E_2 = E_{22} - E_{21}$ [48]. These two equations can be written as the ratio of the lower level:

$$\frac{dN_{22}}{dt} = K^a_p N_1 - K^e_p N_{22} + A^-_{nr} N_{21} - A^+_{nr} N_{22}, \tag{6}$$

$$\frac{dN_{21}}{dt} = M_{12} N_1 - M_{21} N_{21} - N_{21} - 1/\tau - A^-_{nr} N_{21} + A^+_{nr} N_{22}, \tag{7}$$

where the lifetime is $\tau = 1/\gamma$, $K^{a,e}_p$ is absorption and stimulated emission rates of the pump, and $M_{12,21}$ is stimulated absorption and emission rates of the signal. The below formula is then obtained at stationary conditions:

$$\frac{N_{22}}{N} = \frac{\frac{I_p}{b^a_p} + \frac{(I_s + I^{\pm}_{ASE})}{b^a_s}}{(1+\beta)\frac{I_p}{b^a_p} + \beta\frac{I_p}{b^e_p} + (1+\beta+\eta)\frac{(I_s + I^{\pm}_{ASE})}{b^a_s} + 1}. \tag{8}$$

In Eq. (2.8), $b_p^{a,e} = h\nu_p/\tau\sigma_p^{a,e}$, $b_s^{a,e} = h\nu_s/\tau\sigma_s^{a,e}$, I_p and I_s are pump and signal intensity, $I_{ASE}^{\pm}$ is amplified spontaneous emission (ASE) intensity in forward (+) and backward (-) directions, η is the rate between emission and absorption cross-sections, and total concentration distribution of Er^{3+} ions is $N, N = N_1 + N_{21} + N_{22}$ [41–51].

The equations for the propagation of signal, pump, and ASE powers are given as follows:

$$\frac{dP_s}{dz} = 2\pi \int_0^{\infty} I_s[\sigma_s^e N_{21}(r) - \sigma_s^a N_1(r)]rdr, \tag{9}$$

$$\frac{dP_p}{dz} = \pm 2\pi \int_0^{\infty} I_p[\beta\sigma_p^e N_{21}(r) - \sigma_p^a N_1(r)]rdr, \tag{10}$$

$$\frac{dP_{ASE}^{\pm}}{dz} = \pm 2h\nu_s \int_0^{\infty} 2\pi\sigma_s^e N_{21} f_{ASE}^{\pm}(r)rdr \pm 2\pi \int_0^{\infty} [\sigma_s^e N_{21}(r) - \sigma_s^a N_1(r)]P_{ASE}^{\pm} f_{ASE}^{\pm} rdr. \tag{11}$$

$f_{ASE}^{\pm}$ is the normalized ASE profile, and $P_{ASE}^{\pm}$ is ASE power to direction z, which can be defined for both directions ($P_{ASE}^{\pm} = P_{ASE}^{+} + P_{ASE}^{-}$). $f_p(r) \approx f_s(r) \approx f_{ASE}^{+}(r) = f(r)$ and is assumed to spread in the +z direction [43,47,49,50].

With output signal gain for the z = L, the relationship between the amplifier gain and EDF length is:

$$\begin{gathered}\frac{P_s(L)}{P_s(0)} = \exp(-\alpha_s L). \\ \exp\left(\frac{h\nu_s}{P_s^{int}}\left[\frac{P_p(0)-P_p(L)}{h\nu_p} + \frac{(P_s(0)+P_{YKY}^{+}(0))-(P_s(L)+P_{ASE}^{+}(L))}{h\nu_s}\right]\right),\end{gathered} \tag{12}$$

where P_s^{int} is the intrinsic saturation power and its equation is shown below:

$$P_s^{int} = \frac{h\nu_s\ (A_{eff} - 2\tau\sigma_s^e\Gamma)}{\tau\sigma_s^a\Gamma(1+\beta+\eta)}, \tag{13}$$

$$\frac{\nu_p}{\nu_s}\frac{P_s(0)}{P_p(L)}(G-1) + \frac{\sigma_p^a}{\sigma_s^a}\ln(G) = \frac{P_p(0)}{P_p(L)} - 1 - \ln\left(\frac{P_p(0)}{P_p(L)}\right). \tag{14}$$

3. Materials and methods

In this study, each stage of EDF length of a two-stage L-band EDFA with fixed gain, corresponding to changes in wavelength and temperature, is optimized with a GA. Using earlier L-band EDFAs data were analyzed numerically [41]. Figure 2 shows the optimization of a two-stage L-band EDFA.

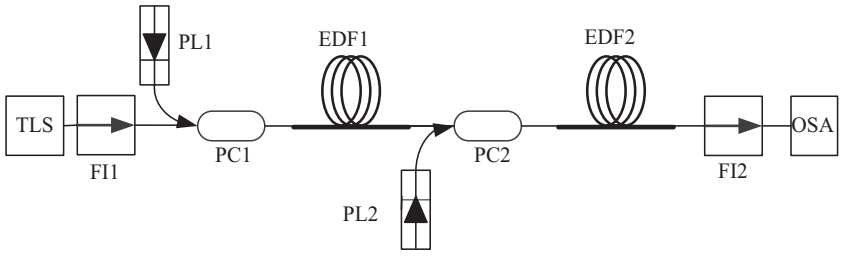

Figure 2. Two-stage L-band EDFA [41].

The input signals are received into a tunable laser source (TLS) that are between 1570 nm and 1610 nm in wavelength and –20 dBm power and pass through port 1 to port 2 of FI1, and then the input and pump signals (PL1) that have 50 mW and 1480 wavelength are combined in a pump coupler (PC1). Following that, these signals are reached as inputs of the co-pumped EDF1, and after that, the amplified signals and second pump signals (PL2) that have same properties as PL1 are combined in PC2, and these signals are given as inputs of the co-pumped EDF2. Finally, two times the amplified signals passing through port 1 to port 2 of FI2 reach the optical spectrum analyzer (OSA). The EDF1 and EDF2 lengths are optimized with a GA in this configuration.

Then the EDF1 and EDF2 lengths optimized with a GA by the temperature of the system are changed between –20 °C and 60 °C. EDF parameter values used in the system are given in the Table.

Table. The parameters of L-band EDFs.

Parameters	Values
Loss at 1300 nm	4 dB/km
Life-time	10 ms
Core radius	1.45 μm
Erbium radius	1 μm
Er^{3+} intensity	9×10^{24} m^{-3}
Numerical aperture	0.24

In the terminology of genetic algorithms, each parameter to be optimized is randomly encoded into binary sequences, which are called a gene, and a set of genes form a chromosome. The quality of an individual in the population with respect to the two objective functions is represented by a scalar value, called fitness. After generating the initial population, each individual is assigned a fitness value. The population is derived again and again, generation by generation, using the crossover operation and the mutation operation. Both operations procreate progeniture by manipulating the individuals in the current population that have good fitness values. The crossover operation exchanges portions of the chromosomes. The mutation operation changes the value of a gene. Individuals with a better fitness value are more likely to survive and to participate in the crossover operation. After a number of generations, the population contains members with better fitness values [52,53]. The model is designed with a GA as shown in Figure 3. As can be seen in this model, the temperature and the total length of the EDF are inputs, and the length of the first and second EDF sections is the output variable. The fitness function is shown below:

First section EDF length = (T+C).0.1 for T = 26, C = –20 °C/+60 °C, where T is base value and C is temperature.

Second section EDF length = (T+C).0.14 for T = 82.5 and C = –20 °C/+60 °C.

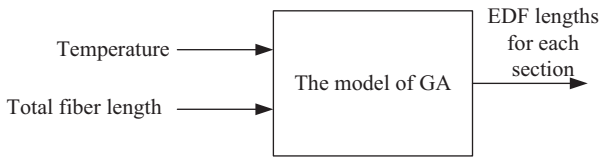

Figure 3. The designed GA model.

For the formulation of the GA model, first the structure of chromosomes must be specified for the first population to be produced. Chromosome structure is composed of temperature and total fiber length. We have

the –20 °C/+60 °C temperature range as mentioned for the model and a total fiber length of between 144.96 and 106.76 m for GA model inputs, and the output is the length of the EDFs.

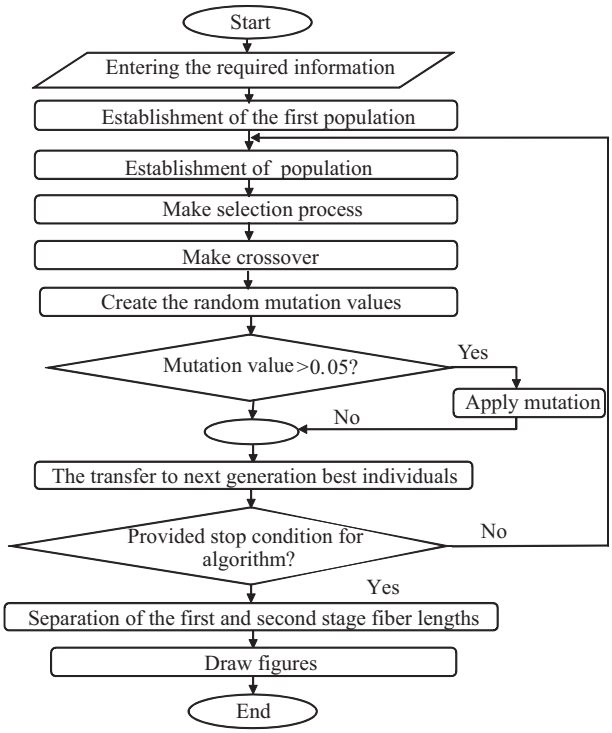

Figure 4. The flowchart of the designed GA model.

The flowchart of the designed GA model is shown in Figure 4. First, as mentioned before, information (temperature, the signal wavelength) is fed into the flow chart as a GA. Then the first population, which consists of the temperature and the EDF length to produce chromosome structure, is formed. Values of temperature between –20 °C and 60 °C are assigned 2–7 bits and converted into the binary system. Values of total EDF lengths between 102 and 112 m are assigned 8–14 bits and then converted to binary system. The selection process among 40 data of the first population is chosen randomly to create the next population. In this study, the "tournament selection rule" by applying the method of selecting the best 20 pairs was randomly selected. It established 20 pairs with a population that was ready for crossover stage. In this study, as a crossing-over method, "uniform crossover" is used for the most relevant results to the theoretical results. After the mutation rate is created randomly, if the mutation value is greater than 0.05 it cannot transfer the next generation of the best members, or else the mutation is applied and transfers to the next generation the best individuals. Then stopping the GA is required. Twenty-two generations are generated, each with a population size of 40, to compare the quality of the fitness functions in this study. The probability of crossover is 0.9 and the probability of mutation is 0.05 in this paper. If EDF lengths for all individuals in the population are between 102 and 112 m, the algorithm is stopped. Thus, the first and second lengths of the EDF lengths are separated. Lastly, the algorithm is terminated by plotting graphs.

4. Results and discussion

The first- and second-stage EDF lengths of a previous theoretical work [41] were optimized by a GA between –20 °C and 60 °C temperature values and the first and second phases respectively are shown in Figures 5 and 6.

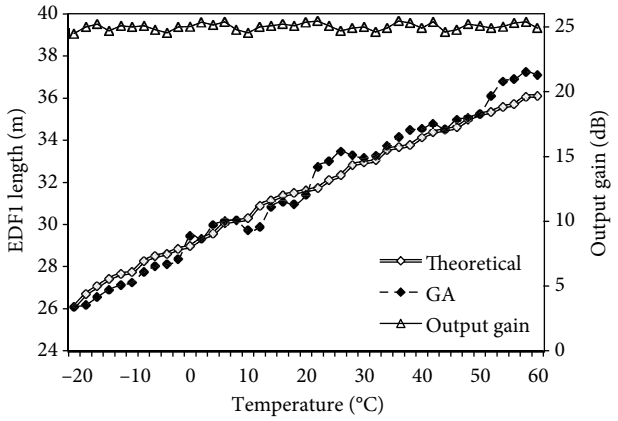

Figure 5. The first-stage EDF length that is found with theoretical work and GA according to changing temperature.

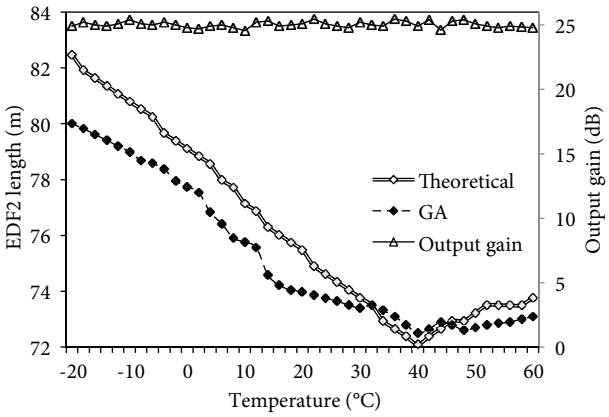

Figure 6. The second-stage EDF length that is found with theoretical work and GA according to changing temperature.

As can be seen in Figure 5, the theoretical and optimized-by-GA EDF length starts at 26 m and differs very little. It is observed that the longer the fiber is, the greater the temperature is. The EDF length of the first stage changes between 26 m and 37 m.

As can be seen in Figure 6, the theoretical and optimized-by-GA EDF length changes in harmony. EDF length of the second stage as the temperature increases up to 40 °C is decreasing, but this is in direct proportion to the slightly increasing temperature value. The output gain is approximate 25 dB for both figures.

In Figure 7, the change in the theoretical and optimized EDF length values depends on the temperature and is drawn as a percentage error for the first stage. As can be seen from the graph, this value varies between –3.5% and 3.5%.

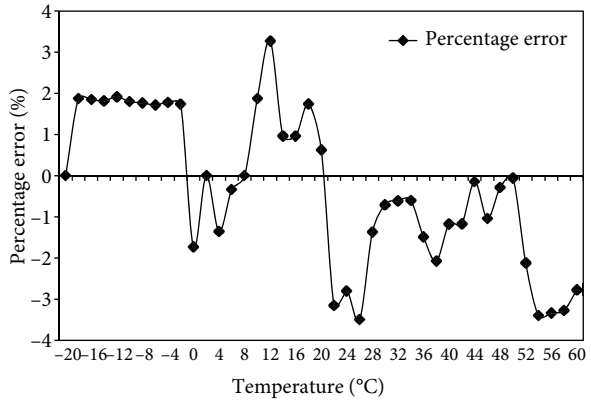

Figure 7. The percent error of theoretical results versus GA results for first-stage fiber length.

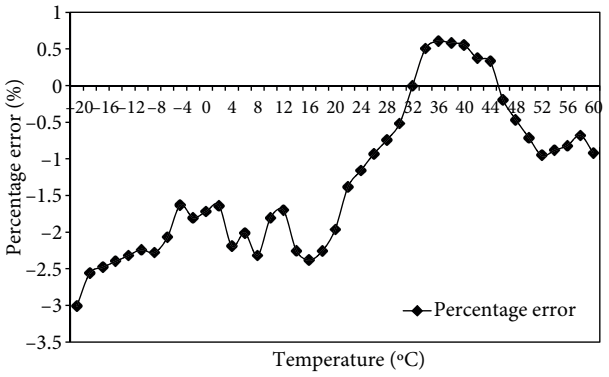

Figure 8. The percent error of theoretical results versus GA results for second-stage fiber length.

The second stage of the length of fiber length values for the theoretical and optimized-by-GA percentage error varies between –3% and 0.5%, as shown in Figure 8. Thus, by using the GA, a rapid, dynamic, high-accuracy model is developed. In addition, different EDFA parameters can be optimized using the GA with a variety of different operating bands. In addition to the C band and the S band, the wavelength of the pump; the first stage, the second stage, or more stages of lengths of fiber; and the gain flattening filters can be optimized using the GA.

5. Conclusions

In this study, the EDF length of the temperature-dependent two-stage L-band EDFA gain is analyzed with the GA approach. EDF length is arranged to obtain accurate values in the range of –20/+60 °C for fixed EDFA gain, which is obtained as 25 dB (±0.5 dB ripple) along the L-band. The users can quite easily define EDF lengths of each stage for the design temperature using this design. The improved GA model shows excellent harmony with the theoretical results for the full spectrum. Classical calculation techniques or experimental setups require enormous computational time and efforts or expensive experimental setups. Contrariwise, the proposed GA approach is very useful for the simple and quick design and simulation of optically related systems under highly temperature-dependent conditions. In addition, this model can be used for different engineering applications and simulations due to the generalization capabilities of GAs.

References

[1] Connelly MJ. Semiconductor Optical Amplifiers. Boston, MA, USA: Kluwer Academic Publishers, 2002.

[2] Yücel M. Design of gain flattened wide band fiber amplifiers. PhD, Gazi University, Ankara, Turkey, 2008.

[3] Mears RJ, Reekie L, Jauncey IM, Payne DN. Low-noise erbium-doped fiber amplifier operating at 1.54 μm. Electron Lett 1987; 23: 1026–1028.

[4] Singh R, Sunanda, Sharma EK. Gain flattening by long period gratings in erbium doped fibers. Optics Comm 2004; 240: 123–132.

[5] Sohn IB, Song JW. Gain flattened and improved double-pass two-stage EDFA using microbending long-period fiber gratings. Optics Comm 2004; 236: 141–144.

[6] Dung S, Chi JC, Wen S. Gain flattening of erbium-doped fibre amplifier using fibre Bragg gratings. Electron Lett 1998; 34: 555–556.

[7] Choi HB, Oh JM, Lee D, Ahn SJ, Park BS, Lee SB. Simple and efficient L-band erbium-doped fiber amplifiers for WDM networks. Optics Comm 2002; 213: 63–66.

[8] Mahdi MA, Sheih SJ. Gain-flattened extended L-band EDFA with 43 nm bandwidth suitable for high signal powers. Optics Comm 2004; 234: 229–233.

[9] Mizuno K, Nishi Y, Mimura Y, Lida Y, Matsuura H, Yoon D, Aso O, Yamamoto T, Toratani T, Ono Y et al. Development of etalon-type gain-flattening filter. Furukawa Review 2000; 19: 53–58.

[10] Yücel M, Göktaş HH. Design of gain flattenned ultra-wideband hybrid optical amplifier. J Fac Eng Archit Gazi Univ 2007; 22: 863–868 (in Turkish with English abstract).

[11] Yücel M, Göktaş HH, Özkaraca O. Temperature dependence of noise figure in the erbium doped fiber amplifier. J Fac Eng Archit Gazi Univ 2010; 25: 635–641 (in Turkish with English abstract).

[12] Yucel M, Goktas HH, Çelebi FV. The effect of pump laser wavelength change on the temperature dependence of EDFA. In: IEEE 19th Signal Processing and Communications Applications Conference; 20–22 April 2011, Antalya, Turkey. New York, NY, USA: IEEE. pp. 238–241.

[13] Yucel M, Goktas HH. Determination of minimum temperature coefficient of C band EDFA. Journal of Applied Sciences 2008; 8: 4464–4467.

[14] Goktas HH, Yucel M. A fuzzy logic based device for the determination of temperature dependence of EDFAs. Microw Opt Techn Let 2008; 50: 2331–2334.

[15] Yucel, M, Aslan Z. The noise figure and gain improvement of double-pass C-band EDFA. Microw Opt Techn Let 2013; 55: 2525–2528.

[16] Yucel M, Aslan Z, Celebi FV, Goktas HH. Gain and noise figure enhancements of both C and L bands double pass erbium doped fiber amplifier. In: ELECO 2013 8th International Conference On Electrical and Electronics Engineering; 28–30 November 2013; Bursa, Turkey. New York, NY, USA: IEEE. pp. 599–603.

[17] Celebi FV. A proposed CAD model based on amplified spontaneous emission spectroscopy. J Optoelectron Adv M 2005; 7: 1573–1579.

[18] Celebi FV, Yucel M, Goktas HH. Fuzzy logic based device to implement a single CAD model for a laser diode based on characteristic quantities. Optik 2012; 123: 471–474.

[19] Celebi FV, Dalkiran I, Danisman K. Injection level dependence of the gain, refractive index variation, and alpha (α) parameter in broad-area InGaAs deep quantum-well lasers. Optik 2006; 117: 511–515.

[20] Çelebi FV, Altindag T, Yildirim R, Gökrem L. Semiconductor laser modeling with ANFIS. In: International Conference on Application of Information and Communication Technologies; 14–16 October 2009; Baku, Azerbaijan. New York, NY, USA: IEEE. pp. 1–4.

[21] Yucel M. Fuzzy logic-based automatic gain controller for EDFA. Microw Opt Techn Let 2011; 53: 2703–2705.

[22] Yigit S, Tugrul B, Celebi FV. A complete CAD model for type-I quantum cascade lasers with the use of artificial bee colony algorithm. Journal of Artificial Intelligence 2012; 5: 76–84.

[23] Celebi FV, Yucel M, Yigit S. Optical gain modelling in type I and type II quantum cascade lasers by using adaptive neuro-fuzzy inference system. In: IEEE 20th Signal Processing and Communications Applications Conference; 18–20 April 2012; Muğla, Turkey. New York, NY, USA: IEEE. pp. 1–4.

[24] Yigit S, Eryigit R, Celebi FV. Optical gain model proposed with the use of artificial neural networks optimised by artificial bee colony algorithm. Optoelectron Adv Mat 2011; 5: 1026–1029.

[25] Celebi FV, Altindag T. An accurate optical gain model using adaptive neurofuzzy inference system. Optoelectron Adv Mat 2009; 3: 975–977.

[26] Celebi FV. A different approach to gain computation in laser diodes with respect to different number of quantum-wells. Optik 2005; 116: 375–378.

[27] Celebi FV, Danisman K. A different approach for the computation of refractive index change in quantum-well diode lasers for different injection levels. P SPIE 2004; 61: 384–388.

[28] Celebi FV. Modeling of the linewidth enhancement factors of the narrow and wide GaAs well semiconductor lasers. J Fac Eng Archit Gazi Univ 2006; 21: 161–166 (in Turkish with English abstract).

[29] Celebi FV, Danisman K. Neural estimator to determine alpha parameter in terms of quantum-well number. Opt Laser Technol 2005; 37: 281–285.

[30] Yildirim R, Celebi FV. The computation of the angle between the gain and photon population by geometrical approach. J Fac Eng Archit Gazi Univ 2009; 24: 709–714 (in Turkish with English abstract).

[31] Tankiz, S, Celebi FV, Yildirim R. Computer-aided design model for a quantum-cascade laser. IET Circ Device Syst 2011; 5: 143–147.

[32] Celebi FV, Yucel M, Goktas HH, Danisman K. Intelligent modelling of alpha (α) parameter; comparison of ANN and ANFIS cases. Optoelectron Adv Mat 2013; 7: 470–474.

[33] Celebi N. A complete type II quantum cascade laser model with the use of RBFN. Optoelectron Adv Mat 2013; 7: 188–190.

[34] Celebi N. An accurate single CAD model based on radial basis function network. Optoelectron Adv Mat 2010; 4: 498–501.

[35] Riziotis C, Vasilakos AV. Computational intelligence in photonics technology and optical networks. Inform Sciences 2007; 177: 5292–5315.

[36] Liu X, Lee B. Optimal design for ultra-broad-band amplifier. J Lightwave Technol 2003; 21: 3446–3455.

[37] Prudenzano F, Mescia L, Orazio A. Optimization and characterization of rare-earth-doped photonic-crystal-fiber amplifier using genetic algorithm. J Lightwave Technol 2007; 25: 2135–2142.

[38] Cheng C, Xiao M. Optimization of an erbium-doped fiber amplifier with radial effects. Optics Comm 2005; 254: 215–222.

[39] Zhang AP, Chen XW, Guan Z, He S, Tam H, Chung W. Optimization of step-changed long-period gratings for gain-flatting of EDFAs. Photonics Technol Lett 2005; 17: 121–123.

[40] Kim H, Bae J, Chun J. Synthesis method based on genetic algorithm for designing EDFA gain flattening LPFGs having phase-shifted effect. Opt Fiber Technol 2009; 15: 320–323.

[41] Yucel M, Goktas HH, Celebi FV. Temperature independent length optimization of L-band EDFAs providing flat gain. Optik 2011; 122: 872–876.

[42] Yamada M, Schimizu M, Horiguchi M, Okayasu M. Temperature dependence of signal gain in Er^{3+}-doped optical fiber amplifiers. IEEE J Quantum Elect 1992; 28: 640–649.

[43] McCumber DE. Theory of phonon-terminated optical masers. Phys Rev 1964; 134: A299–A305.

[44] Kagi N, Oyobe A, Nakamura K. Temperature dependence of the gain in erbium doped fibers. J Lightwave Technol 1991; 9: 261–265.

[45] Kemtchou J, Duhamel M, Lecoy P. Gain temperature dependence of erbium-doped silica and fluoride fiber amplifiers in multichannel wavelength-multiplexed transmission systems. J Lightwave Technol 1997; 15: 2083–2090.

[46] Bolshtyansky M, Wysocki P, Conti N. Model of temperature dependence for gain shape of erbium-doped fiber amplifier. J Lightwave Technol 2000; 18: 1533–1540.

[47] Desurvire E. Erbium-Doped Fiber Amplifiers: Principles and Applications. New York, NY, USA: John Wiley, 1994.

[48] Aozasa S, Sakamoto T, Ono H, Mori A, Yamada M. Wideband rare-earth-doped fiber amplification technologies – O and S band amplification technologies. NTT Technical Review 2004; 2: 44–50.

[49] Lin MC, Chi S. The gain and optimal length in the erbium-doped fiber amplifiers with 1480 nm pumping. Photonics Technol Lett 1992; 4: 354–356.

[50] Kogelnick H, Yariv A. Considerations of noise and schemes for its reduction in laser amplifiers. P IEEE 1964; 52: 165–172.

[51] Berkdemir C, Özsoy S. The temperature dependent performance analysis of EDFAs pumped at 1480 nm: a more accurate propagation equation. Opt Express 2005; 13: 5179–5185.

[52] Yang HS, Martin M, Reisslein M, Carlyle WM. A genetic algorithm-based methodology for optimizing multiservice convergence in a metro WDM network. J Lightwave Technol 2003; 21: 1114–1133.

[53] Cheng C, Xu Z, Sui C. A novel design method: a genetic algorithm applied to an erbium-doped fiber amplifier. Optics Comm 2003; 227: 371–382.